J. Phys. B: Atom. Molec. Phys., Vol. 11, No. 22, 1978. Printed in Great Britain

Differential and integral cross sections for the electron impact excitation of O_2 I. Optically allowed transitions from the ground state

K Wakiya

Department of Physics, Faculty of Science and Technology, Sophia University, Chiyoda-ku, Tokyo 102, Japan

Received 8 March 1978, in final form 26 June 1978

Abstract. Electron energy-loss spectra of O_2 have been analysed for incident electron energies from 20 to 500 eV, scattering angles from 5 to 130°, and energy losses from 4 to 12·1 eV. Differential and integral cross sections for excitation of the Schumann–Runge continuum, for excited states ranging from 9·7 to 12·1 eV of energy loss, and for elastic scattering have been determined. For the Schumann–Runge continuum oscillator strengths have been calculated from the data. Integral cross sections for the Schumann–Runge continuum as a function of impact energy are compared to theoretical calculations. Differential cross sections for electrons elastically scattered by O_2 in the 200–500 eV impact energy range agree well with the observed values by Bromberg and with calculations utilising the independent-atom mode. Excitations to the excited states in the range of 9·7–12·1 eV of energy loss are found to be due mainly to the optically allowed transitions. This designation was deduced by the angular distribution and energy dependence of the differential cross sections.

1. Introduction

Oxygen, the second most abundant molecule next to nitrogen in the atmosphere, plays an important role in atmospheric chemistry and physics. The spectrum of energy absorption by O_2 has been studied optically by many workers. The results have been critically reviewed by Hudson (1971) and Krupenie (1972). The Schumann–Runge continuum is an optically allowed transition and is very intense. There are two strong bands (longest band, second band) and many weak features corresponding to higher excitation energies which appear in optical spectra.

Geiger and Schröder (1968) obtained electron impact energy-loss spectra of O_2 at 25 keV impact energy and zero scattering angle. Under these conditions the electron impact spectrum is essentially identical with the photoabsorption spectra. They compared the resulting energy-loss spectrum with the UV absorption spectrum. At energies of 50, 70 and approximately 500 eV and at low scattering angles (below 14°) Lassettre *et al* (1964b, 1968) measured the energy-loss spectrum for the Schumann–Runge continuum (SR continuum) and excited states ranging from 9·94 to 30 eV energy loss.

Trajmar *et al* (1972) determined the angular behaviour of the differential cross section for excitation of the B $^3\Sigma_u^-$ state, for the longest band and the second band

0022-3700/78/0022-3913 $03.00

transitions, and for elastic scattering at 20 and 45 eV impact energies and at scattering angles ranging from 20 to 90°. Cartwright *et al* (1973) observed discrete bands in the electron impact energy-loss spectrum of O_2 superimposed on the SR continuum, and with the help of theoretical calculations assigned them to the $3s\sigma_g\ ^3\Pi_g$ Rydberg state. Recently Cartwright *et al* (1976) reported a quantitative decomposition of the SR continuum. Very recently Trajmar *et al* (1976) observed electron impact energy-loss spectra of O_2 in the 7–10 eV region at low impact energies and high scattering angles, and found a number of new transitions which do not appear in optical spectra.

Differential cross sections (DCS) and integral cross sections for excitation of the SR continuum, for excited states ranging from 9·7 to 12·1 eV energy loss, and for elastic scattering are reported here in the impact energy range from 20 to 500 eV, and for scattering angles from 3 to 130°. This is the first investigation which determines the cross section systematically for a wide intermediate energy region and a wide angular range. The experimental methods and the normalisation procedure to determine the absolute scale are discussed, and a comparison between these cross sections and the calculated values or measured ones by Trajmar *et al* (1971, 1972) is made.

2. Apparatus and experimental methods

The instrument used in the present measurements is the same as that used over the past few years in the measurement of the DCS for excitation in He by Takayanagi (1973), Suzuki *et al* (1974) and Yagishita *et al* (1976). The electron impact spectrometer consists of three parts: a beam source of monoenergetic electrons, a sample cell (collision chamber) for the static gas target and an energy analyser with a channel electron multiplier. A schematic diagram of the apparatus is shown in figure 1.

The energy selector and analyser are both of the hemispherical electrostatic type, with mean radii of 30 mm.

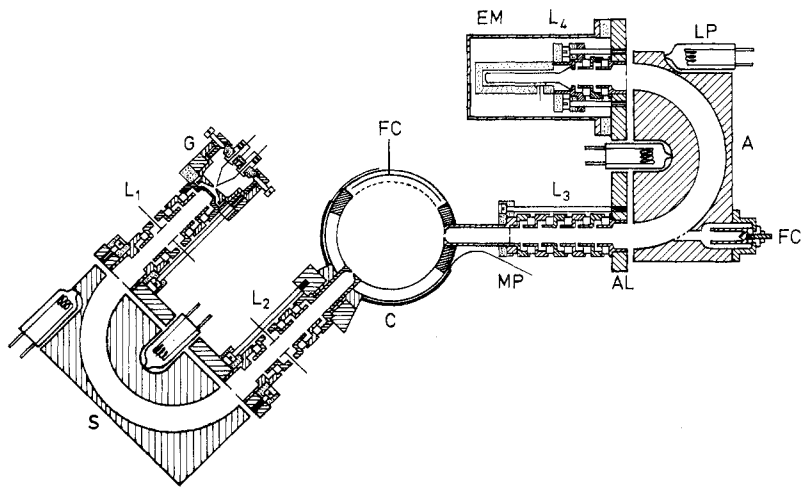

Figure 1. Schematic diagram of the experimental apparatus. G: electron gun; L_1, L_2, L_3, L_4: electron optics system; S: selector; C: collision chamber; MP: sliding molybdenum plate; FC: Faraday cup; AL: the entrance and exit plane of the analyser; A: analyser; EM: electron multiplier; LP: halogen lamp for baking.

An electron beam from a Pierce-type electron gun with a hairpin tungsten cathode enters the energy selector at about 2 eV kinetic energy. Electrons pass through a space between the hemisphere and are dispersed according to their kinetic energy. Electrons emerging from the selector with kinetic energy within a narrow range are accelerated to the desired impact energy (E_0) and are focused into the collision chamber which contains the gaseous molecular target at a pressure of about 10^{-5}–10^{-3} Torr. Electrons that lose a certain amount of energy (W) and undergo scattering by a specific angle (θ) are passed by the energy analyser and are detected.

Voltages on all elements of L_3 and L_4 of the electrostatics lens system for the analyser are applied against the entrance and exit electrode AL of the analyser. The voltage on AL is swept as a function of energy lost by the scattered electron. An important feature of the lens system L_3 is that the transmission of the optics should be independent of the kinetic energy of the scattered electrons. By virtue of these lens optics, we may then obtain relative peak intensities in the energy-loss spectra correctly proportional to the DCS for the respective scatterings.

The collision chamber C in figure 1 is designed to keep the pressure of sample gas constant when the scattering angle is changed continuously. The slot in the cylinder is covered with a thin molybdenum plate MP, which is fixed to the selector system and slides smoothly in contact with the side of the cylinder. This collision chamber achieves an angular range from -5 to $+130°$ by rotating the selector system around the collision centre in a plane containing the incident beam. It maintains a pressure in the collision chamber at least several hundred times the pressure in the main chamber. A Faraday cup FC is mounted along the inner surface of the collision chamber in order to absorb the incident electron beam and monitor its intensity.

All electron optics, slits and apertures are made of molybdenum. The hemispheres and the holders are made of stainless steel. The spectrometer is bakable up to about 150°C using the halogen lamps LP. External magnetic fields are attenuated to about 0·5–2 mG by two layers of Permalloy magnetic shield and a pair of Helmholtz coils.

We have made most of the measurements in the range of intermediate impact energies at a resolution of about 200 meV FWHM in the energy-loss spectrum. A resolution as good as 50 meV was obtained without difficulty; however, the most preferable conditions for practical measurements were given for 200 meV resolution. An angular resolution of about $\pm 2°$ is estimated from the geometrical structure of the apparatus.

3. Normalisation to determine the absolute scale

3.1. Elastic scattering cross section

First the angular dependence of the elastic scattering intensity $I_{\text{elas}}(\theta)$ is determined. The relative elastic DCS at θ is given by

$$\left(\frac{\mathrm{d}\sigma_{\text{elas}}}{\mathrm{d}\Omega}\right)_{\text{r}} = I_{\text{elas}}(\theta)\sin\theta \tag{1}$$

where $\sin\theta$ is the correction factor for the variation of the 'effective path length' as a function of θ.

The relative elastic DCS curve was extrapolated to angles smaller than 10° and larger than 130°. Then the relative integral cross section for elastic scattering

$$\sigma^{r}_{elas}(E_0) = 2\pi \int_{0°}^{180°} \left(\frac{d\sigma_{elas}}{d\Omega}\right)_r \sin\theta \, d\theta \tag{2}$$

is calculated.

The relative elastic DCS at 300, 400 and 500 eV have been normalised to the absolute scale of the elastic DCS by Bromberg (1974) at $\theta = 30°$.

The relative elastic DCS at 20–100 eV have been normalised to the absolute scale by the procedure as follows:

$$\sigma_{tot} = C(\sigma^{r}_{elas} + \Sigma\sigma^{r}_{elec}) + \sigma_{ion} + \Sigma\sigma_{vib} \tag{3}$$

$$\sigma_{elas} = C\sigma^{r}_{elas} \tag{4}$$

$$\left(\frac{d\sigma_{elas}}{d\Omega}\right) = C\left(\frac{d\sigma_{elas}}{d\Omega}\right)_r. \tag{5}$$

In equation (3), σ_{tot} is the absolute total cross section, $\Sigma\sigma^{r}_{elec}$ is the sum of the relative integral cross section for all electronic excitations; σ_{ion} and $\Sigma\sigma_{vib}$ are the absolute integral ionisation cross section and the sum of the vibrational one, respectively. In equations (4) and (5), the cross sections are then placed on an absolute scale by determining the normalising constant C from equation (3).

For $E_0 = 150$ and 200 eV, the relative σ^{r}_{elas} are normalised by a linear interpolation of the deduced σ_{elas} at $E_0 = 100$ eV and the absolute σ_{elas} at $E_0 = 300$, 400 and 500 eV.

3.2. Inelastic scattering cross section

For scattering angles from 10 to 130°, the ratio of the excitation cross section to the elastic one is obtained from the electron energy-loss spectrum. A typical spectrum is shown in figure 2. From each spectrum we obtain the ratio $R_n(\theta) = S_n(\theta)/S_{elas}(\theta)$, where $S_n(\theta)$ and $S_{elas}(\theta)$ are the area under the peak associated with the excitation for the electronic state n and the area under the elastic scattering peak, respectively. For the electronic states n the DCS is given by the following relation

$$\left(\frac{d\sigma_n}{d\Omega}\right) = R_n(\theta)\left(\frac{d\sigma_{elas}}{d\Omega}\right). \tag{6}$$

For small scattering angles below 10°, we were afraid that the spectrometer used could not completely distinguish the elastically scattered electrons from the directly injected ones due to the low angular resolution. To obtain the DCS for the SR continuum in the range of 3–30°, we have used a method of mixing He with O_2, instead of the procedure which was described in the previous paragraph. The energy-loss spectra of the gas mixture, where the relative partial pressures were known, have been measured in the range of scattering angle 3–30° and for incident electron energies from 150 to 500 eV covering the range of 4–25 eV energy loss.

If the analyser A is operated in the constant-resolution mode, the DCS for the SR continuum at the small (below 10°) and large scattering angles is given by the

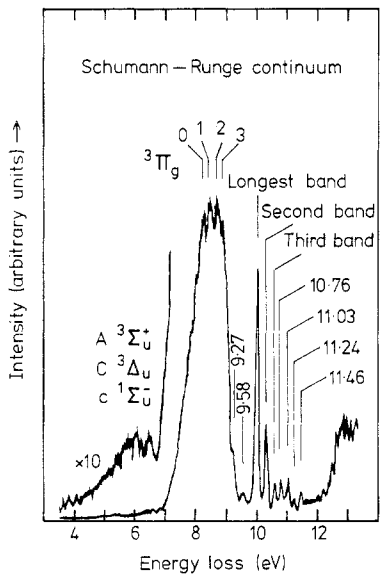

Figure 2. Electron impact energy-loss spectrum of O_2. Impact energy E_0 = 50 eV, scattering angle θ = 15°, energy-loss region 3·5–13·4 eV.

following relation (Lassettre *et al* 1964a, 1966)

$$\left(\frac{d\sigma_{SR}}{d\Omega}\right) = \frac{P_{He}}{P_{O_2}} \frac{S_{SR}(\theta)}{S_{2^1P}(\theta)} \left(\frac{d\sigma_{2^1P}}{d\Omega}\right) \tag{7}$$

where P_{He} and P_{O_2} are the partial pressure of He and O_2 in the collision chamber, respectively; $S_{SR}(\theta)$ and $S_{2^1P}(\theta)$ are the areas under the respective peaks in the energy-loss spectrum of O_2 (SR continuum) and He(2^1P); $(d\sigma_{2^1P}/d\Omega)$ is the DCS for the He(2^1P). The ratio P_{He}/P_{O_2} was deduced from the observed values of $(d\sigma_{SR}/d\Omega)$, $S_{SR}(\theta)/S_{2^1P}(\theta)$ and $(d\sigma_{2^1P}/d\Omega)$ at E_0 = 500 eV and θ = 15°. For $(d\sigma_{SR}/d\Omega)$, the value which was determined with pure O_2 gas was used. Once P_{He}/P_{O_2} was determined, this value was used at other energies and scattering angles.

4. Results and discussions

4.1. DCS for elastic scattering

The elastic scattering DCS (E_0 = 20–100 eV, θ = 10–130°) shown in figures 3(*a*) and (*b*) were obtained from the procedures described in §3.1. For σ_{tot} in equation (3) we utilised the total scattering cross section measurements of Salop and Nakano (1970) at E_0 = 20 eV, and of Sunshine *et al* (1967) in the 30–100 eV range. For σ_{ion} in equation (3) we utilised the total ionisation cross section determined by Rapp and Englander-Golden (1965) in the 20–100 eV range.

For pure vibrational excitation cross section, σ_{vib} in equation (3), the experimental values by Trajmar *et al* (1972) were used; although σ_{vib}(20 eV) was available for their results, σ_{vib}(30 eV) was obtained by an interpolation between the results at 20 and 45 eV; for σ_{vib}(50 eV) we used the data for 45 eV. The integral cross sections used for the normalisation in the present work are given in table 1.

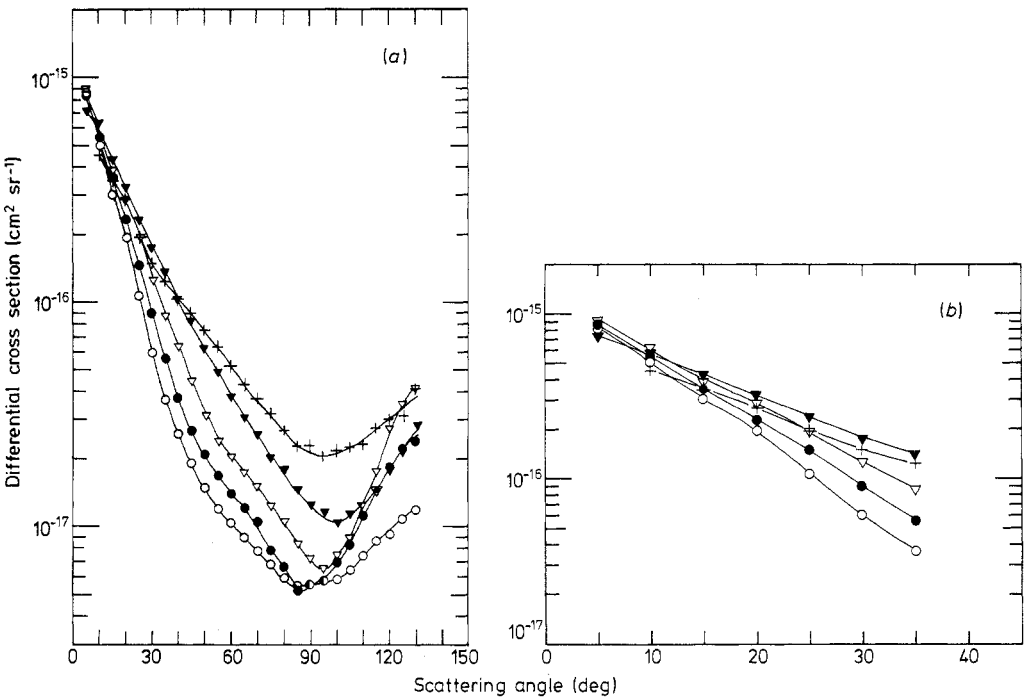

Figure 3. (*a*) The DCS of electrons elastically scattered by O_2 at different incident electron energies: + 20 eV, ▼ 30 eV, ▽ 50 eV, ● 70 eV, ○ 100 eV. The symbol ▼ means that ▼ and ▽ have the same value and the symbol ◐ is similar but for ● and ○. (*b*) As (*a*), except that the scale of the scattering angle is extended four times in the range of θ = 5–35°.

As shown in figures 3(*a*) and (*b*), the shape of the measured angular distribution is characterised by nearly exponential behaviour in the two angular ranges 10–80° and 100–130°. The forward-peaking slope of the elastic DCS for scattering angles smaller than about 40° increases monotonically as the incident energy increases. On the other hand, the backward-peaking slope in the angular dependence has a maximum near 50 eV incident energy and decreases for both higher and lower energies. Moreover, the scattering angle where the cross sections show their minima in the curve are found to be around 85–100° somewhat depending on energy. The minimum cross section tends to decrease as the incident energy increases.

Very few data are available for the elastic DCS in O_2 in the energy region lower than 100 eV. A comparison of the present results with elastic DCS (O_2) by Trajmar *et al* (1971, 1972) at E_0 = 20 and 45 eV will be given in the following section.

In figures 4(*a*)–(*c*), the experimental DCS (E_0 = 100–500 eV, θ = 10–130°) which were obtained by the procedures described in §3.1 are shown. Experimental results of Bromberg (1974) in the 300–500 eV range and theoretical calculations of Hayashi (1975) and Hayashi and Kuchitsu (1976) and H Daimon (1977, private communication) at 100–500 eV are also shown on the figures for comparison. The calculations by Hayashi and Daimon were obtained by means of the independent-atom model, using the multiple-scattering effect which is expressed by a sum of one-centre long-range potentials and multi-centre short-range potentials.

As shown in figures 4(*b*) and (*c*), the present results show quite good agreement with experimental data by Bromberg and calculations by Hayashi for electron

Table 1. Integral cross sections (cm^2) used for normalisation of experimental data and deduced integral cross sections (σ_a, σ_b, σ_{ACc}, σ_{SR}, σ_W and σ_{elas}).

Impact energy E_0(eV)			20	30	50	70	100	Reference
Data used for normalisation	Total	σ_{tot}	$9{\cdot}4 \times 10^{-16}$	$9{\cdot}3 \times 10^{-16}$	$9{\cdot}3 \times 10^{-16}$	$7{\cdot}7 \times 10^{-16}$	$6{\cdot}7 \times 10^{-16}$	a, b
	Ionisation	σ_{ion}	$3{\cdot}07 \times 10^{-17}$	$8{\cdot}98 \times 10^{-17}$	$1{\cdot}88 \times 10^{-16}$	$2{\cdot}34 \times 10^{-16}$	$2{\cdot}68 \times 10^{-16}$	c
	Vibration	$\Sigma\sigma_{vib}$	$4{\cdot}0 \times 10^{-18}$	$2{\cdot}9 \times 10^{-18}$	$1{\cdot}3 \times 10^{-18}$			d
Result	a $^1\Delta_g$	σ_a	$3{\cdot}24 \times 10^{-18}$	$3{\cdot}08 \times 10^{-18}$	$1{\cdot}58 \times 10^{-18}$	$5{\cdot}59 \times 10^{-19}$	$2{\cdot}15 \times 10^{-19}$	e
	b $^1\Sigma_u^+$	σ_b	$1{\cdot}01 \times 10^{-18}$	$9{\cdot}77 \times 10^{-19}$	$6{\cdot}46 \times 10^{-19}$	$1{\cdot}78 \times 10^{-19}$	$4{\cdot}90 \times 10^{-20}$	e
	A $^3\Sigma_u^+$ + c $^3\Delta_u$ + c $^1\Sigma_u^-$	σ_{ACc}	$1{\cdot}00 \times 10^{-17}$	$6{\cdot}06 \times 10^{-18}$	$5{\cdot}11 \times 10^{-18}$	$2{\cdot}06 \times 10^{-18}$	$1{\cdot}06 \times 10^{-18}$	e
	SR continuum	σ_{SR}	$9{\cdot}50 \times 10^{-17}$	$7{\cdot}83 \times 10^{-17}$	$6{\cdot}94 \times 10^{-17}$	$5{\cdot}50 \times 10^{-17}$	$4{\cdot}95 \times 10^{-17}$	f
	$W = 9{\cdot}7$–$12{\cdot}1$	σ_W	$1{\cdot}57 \times 10^{-17}$	$1{\cdot}53 \times 10^{-17}$	$1{\cdot}36 \times 10^{-17}$	$8{\cdot}95 \times 10^{-18}$	$7{\cdot}65 \times 10^{-18}$	f
	Elastic	σ_{elas}	$7{\cdot}80 \times 10^{-16}$	$7{\cdot}34 \times 10^{-16}$	$6{\cdot}50 \times 10^{-16}$	$4{\cdot}69 \times 10^{-16}$	$3{\cdot}44 \times 10^{-16}$	f

[a] $E_0 = 20$ eV: Salop and Nakano (1970); relative error $\pm$ 10%.
[b] $E_0 = 30$–100 eV: Sunshine *et al* (1967); relative error $\pm$ 20%.
[c] Rapp and Englander-Golden (1965); relative error $\pm$ 10%.
[d] Trajmar *et al* (1972).
[e] Wakiya (1978).
[f] Present work.

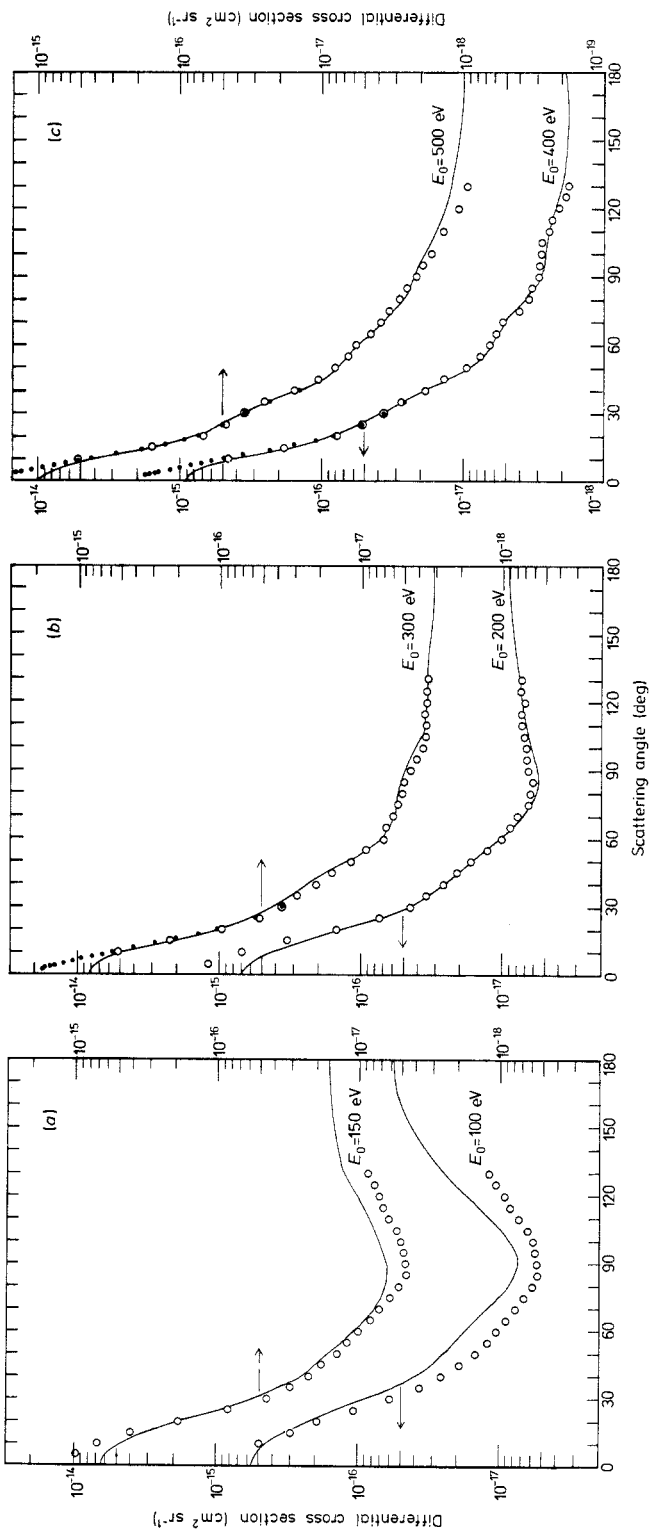

Figure 4. The DCS of electrons elastically scattered by O_2 at different incident electron energies; (*a*) 100 and 150 eV, (*b*) 200 and 300 eV, (*c*) 400 and 500 eV. Large open circles O indicate present results, which were used as standards for normalising the excitation cross section. In (*b*) and (*c*), small closed circles • represent experimental data of Bromberg (1974). The curves at E_0 = 150 500 eV and one at E_0 = 100 eV are calculated by Hayashi (1975) and Hayashi and Kuchitsu (1976) and H Daimon (1977, private communication), respectively.

Table 2. Summary of the recently published DCS of electrons elastically scattered by O_2.

Workers	E_0(eV)	θ(deg)	Comments
Trajmar *et al* (1971, 1972)	20, 45	10–90	Normalised DCS
Hayashi (1975)	100–500	10–60	Normalised DCS
Bromberg (1974)	300, 400, 500	2–40	Absolute DCS
Hayashi (1975)	150–500	0–180	Theoretical DCS
Daimon (1977, private communication)	100	0–180	Theoretical DCS
Present work	20–500	10–130	Normalised DCS

energies above 200 eV. At smaller scattering angles, theoretical values yield smaller cross sections than the experimental ones. The reason for this is that the polarisation effect has not been taken into account in the calculation.

As can be seen in figure 4(*a*), at E_0 = 100 and 150 eV the present results give, on the whole, smaller cross sections than the calculated results of Hayashi (1975) and Hayashi and Kuchitsu (1976), Daimon (1977, private communication). It is considered that the accuracy of their calculated values might not be too accurate at low impact energy (below 150 eV) while our data contain errors caused by the normalisation to the absolute scale. However, the present data are in agreement with the calculated ones within the estimated errors given in table 3.

A summary of the published elastic DCS is given in table 2. The percentage errors included in the present work (elastic DCS) are given in table 3. These errors in the E_0 = 20–150 eV range are considered to be mostly due to the systematic errors in the previous work from which we took out the normalisation standards for our absolute scale.

Table 3. Estimated percentage errors in the DCS and the integral cross sections for elastic scattering.

E_0(eV)	20	30	50	70	100	150	200	300–500
Normalisation[a]	11	23	28	33	40	33	5	3
Statistical[b]	7	6	5	5	5	5	5	5
Extrapolation[b]	3	2	2	2	2	2	2	1
Total (%)	13	24	29	33	40	34	7	6

[a] Errors introduced by other workers.
[b] Errors of present work.

4.2. DCS for inelastic scattering

4.2.1. Schumann–Runge continuum. In the typical electron impact energy-loss spectrum of O_2 shown in figure 2, the intense continuum with a broad maximum at 8·6 eV is the well known Schumann–Runge continuum. On the high-energy side of the continuum one shoulder is observed at approximately 9·27 eV along with a broad peak at 9·58 eV in agreement with the data of Watanabe *et al* (1953). The region above the SR continuum will be discussed later in §4.2.3. The continuum with a broad peak at 6·1 eV below the SR continuum is designated as the transition ($A\,^3\Sigma_u^+ + c\,^3\Delta_u + c\,^1\Sigma_u^- \leftarrow X\,^3\Sigma_g^-$. The angular behaviour of the DCS and integral cross sections for excitation of these bands for E_0 = 20–500 eV has been determined by Wakiya (1978).

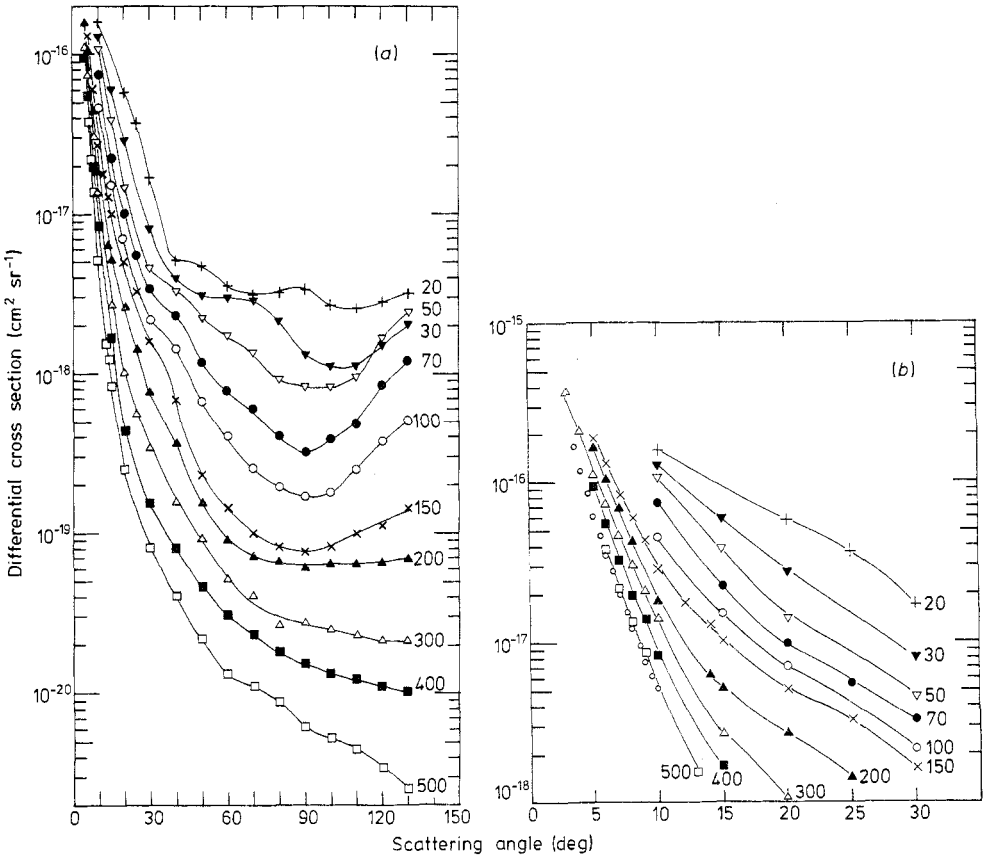

Figure 5. (*a*) The DCS for excitation of the Schumann–Runge continuum in O_2 at different incident electron energies: + 20 eV, ▼ 30 eV, ▽ 50 eV, ● 70 eV, ○ 100 eV, × 150 eV, ▲ 200 eV, △ 300 eV, ■ 400 eV and □ 500 eV. (*b*) As (*a*), except that the scale of scattering angle is extended four times in the range of $\theta = 3$–$30°$. Small open circles ◦ indicate the corrected DCS of Lassettre and Francis (1964), which are multiplied by 0·77 since their data were considered to contain the streaming error in a McLeod gauge (Lassettre *et al* 1971), $E_0 = 519$ eV.

The DCS for excitation of the SR continuum at incident energies from 20 to 500 eV are shown in figures 5(*a*) and (*b*). The DCS were determined by the procedures described in § 3.2 with pure O_2 gas at scattering angles ranging from 10 to 130°, and by mixing He with O_2 at scattering angles ranging from 3 to 30°. Since the angular distribution of the DCS obtained using mixed gases are in agreement with that obtained with pure gas at the overlapped scattering angles ranging from 10 to 30°, we have taken the average values of the DCS by these two methods. To obtain the area $S_{SR}(\theta)$ under the broak peak of the SR continuum, the lower and the upper limit of the energy-loss region have been taken to be 7·1 eV and 9·7 eV, respectively.

For the DCS of the He(2^1P) in equation (7), we have used theoretical values by Kim and Inokuti (1968) in the scattering angle from 3 to 9°, and averages of the experimental data of Dillon and Lassettre (1975), Takayanagi (1973) and Suzuki *et al* (1974) in the scattering angle from 10 to 30°.

As can be seen in figures 5(*a*) and (*b*), the forward-peaking slope of the DCS for the SR continuum increases monotonically as the incident energy increases, while

the slope of the backward region has a maximum near 50 eV incident energy and decreases for both higher and lower energies. Moreover, at the impact energies below 150 eV, a minimum is found around 90–110° and this moves to larger angles as the collision energy decreases.

For impact energies above 200 eV, the DCS of the SR continuum for the large scattering angles (above 60°) decreases as the impact energy and the scattering angle increase. A slight undulation is seen in the angular distribution at angles between 30 and 60° for collision energies 50–150 eV. Another small undulation appears around 60–90° for the 20 and 30 eV range. The angular dependence of the DCS for the SR continuum shows larger slopes than that of the elastic scattering at the same small scattering angle and at the same impact energy. For example, at $E_0 = 500$ eV the $DCS_{SR}(10°)/DCS_{SR}(20°)$ is about 20·4, while the $DCS_{elas}(10°)/DCS_{elas}(20°)$ is about 7·6.

The results of Lassettre *et al* (1964b) at $E_0 = 519$ eV are also shown in figure 5(*b*) for comparison. Their results are corrected by multiplying by 0·77 since these were considered to contain the streaming error of a McLeod gauge (Lassettre and Skerbele 1971). The angular distribution of the present work at $E_0 = 500$ eV is in good agreement with their results.

There remains three main problems in obtaining the cross sections for the SR continuum. The first problem is the choice of the lower energy limit, because the 6·1 eV bands and the SR continuum cannot be separated in the energy-loss spectrum. We determined the limit to be 7·1 eV because it is the dissociation limit of the B $^3\Sigma_u^-$ state.

The second problem is the choice of the upper energy limit of 9·7 eV (the minimum point between the 9·58 eV peak and the longest band) because the SR continuum, 9·58 peak and longest band at 9·96 eV were not completely resolved. However, the magnitude of the cross section for the SR continuum varies by only about 1% due to the choice of this integration limit.

The third problem is the effect of double scattering at large momentum transfer in the optically allowed transition (Chamberlain *et al* 1967, Lassettre and Francis 1964). We measured the pressure dependence of the energy-loss spectra and corrected for the effects of double scattering on the DCS at large momentum transfers.

The percentage errors in the present DCS measurement for the SR continuum are given in table 4.

Table 4. Estimated percentage errors in the DCS and the integral cross sections for the Schumann–Runge continuum.

E_0(eV)	20	30	50	70	100	150	200	300–500
Normalisation[a]	11	23	28	33	40	33	5	3
Statistical[b]	14	13	7	9	10	10	10	13
Extrapolation[b]	3	3	3	3	3	2	2	2
Elastic[b]	7	6	5	5	5	5	5	5
Total (%)	19	27	29	34	42	35	12	14

[a] Errors introduced by other workers.
[b] Errors of present work.

4.2.2. Generalised oscillator strength for the Schumann–Runge continuum. To investigate to what extent the Born approximation holds as the impact energy decreases and to test the accuracy of the DCS for the SR continuum, the generalised oscillator

strength f was obtained from the measured DCS. The generalised oscillator strength (GOS) f was introduced by Bethe (1930) to establish the close connection between the excitation of atoms and molecules by electron impact and the excitation produced by absorption of electromagnetic radiation. GOS f is defined in atomic units (au) as follows

$$f = \frac{W}{2}\frac{P_1}{P_2}\left(\frac{\mathrm{d}\sigma}{\mathrm{d}\Omega}\right)(\Delta P)^2 \qquad \text{(discrete spectrum)} \tag{8a}$$

$$\left(\frac{\mathrm{d}f}{\mathrm{d}W}\right) = \frac{W}{2}\frac{P_1}{P_2}\left(\frac{\mathrm{d}^2\sigma}{\mathrm{d}\Omega\,\mathrm{d}W}\right)(\Delta P)^2 \qquad \text{(continuous spectrum)} \tag{8b}$$

where W is the excitation energy; P_1 and P_2 are the momentum vectors for the incident and the scattered electrons, respectively; $(\Delta P)^2$ is the square of the momentum change of the colliding electron, that is,

$$(\Delta P)^2 = P_1^2 + P_2^2 - 2P_1P_2\cos\theta$$

where θ is the scattering angle; $(\mathrm{d}\sigma/\mathrm{d}\Omega)$ is the DCS per unit solid angle for excitation of the atom or molecule; $(\mathrm{d}^2\sigma/\mathrm{d}\Omega\,\mathrm{d}W)$ is doubly differential cross section per unit solid angle and per unit excitation energy for excitation of an atom or molecule.

The f values deduced from experimental DCS using equation (8*a*) or (8*b*) are called sometimes the effective (or apparent) oscillator strength.

The generalised oscillator strength f_{SR} for the overall SR continuum region at a specific scattering angle can be calculated by the following relation

$$f_{SR} = \int_{\text{peak}}\left(\frac{\mathrm{d}f}{\mathrm{d}W}\right)\mathrm{d}W = \int_{\text{peak}}\frac{W}{2}\frac{P_1}{P_2}\left(\frac{\mathrm{d}^2\sigma}{\mathrm{d}\Omega\,\mathrm{d}W}\right)(\Delta P)^2\,\mathrm{d}W. \tag{8c}$$

If $E_0 \gg W$, equation (8*c*) can be approximated as follows

$$f_{SR} = \left[\frac{W}{2}\frac{P_1}{P_2}(\Delta P)^2\right]_{W=8{\cdot}44\text{ eV}}\int_{\text{peak}}\left(\frac{\mathrm{d}^2\sigma}{\mathrm{d}\Omega\,\mathrm{d}W}\right)\mathrm{d}W$$

$$= \left[\frac{W}{2}\frac{P_1}{P_2}(\Delta P)^2\right]_{W=8{\cdot}44\text{ eV}}\left(\frac{\mathrm{d}\sigma}{\mathrm{d}\Omega}\right)_{SR}. \tag{8d}$$

In figure 6, the f_{SR} deduced from the present $(\mathrm{d}\sigma/\mathrm{d}\Omega)_{SR}$ using equation (8*d*) are shown as a function of $(\Delta P)^2$. If the Born approximation is obeyed the data for all impact energies from 150 to 500 eV should lie on the same curve. This is nearly satisfied for 300, 400 and 500 eV impact energies in the small $(\Delta P)^2$ region below about 2·0 (au). As the impact energy decreases from 300 to 150 eV, f_{SR} decreases to depart from the curve of the ideal GOS. For large $(\Delta P)^2$ above 2·0 (au), f_{SR} increases monotonically as the impact energy decreases. The behaviour of f_{SR} as a function of $(\Delta P)^2$ has a tendency to flatten on the whole as the impact energy decreases. The corrected GOS (i.e. corrected for streaming effect; see § 4.2.1) of Lassettre *et al* (1964b) at $E_0 = 519$ eV are also shown in figure 6 for comparison. The GOS of the present work at $E_0 = 400$ and 500 eV are in good agreement with the results of Lassettre *et al* (1964b).

For the value of the optical oscillator strength f_0 for the SR continuum we chose $f_0 = 1{\cdot}61$ from Watanabe *et al* (1953). This value is in good agreement with the extrapolated value of the present oscillator strength curves through data to $(\Delta P)^2 = 0$.

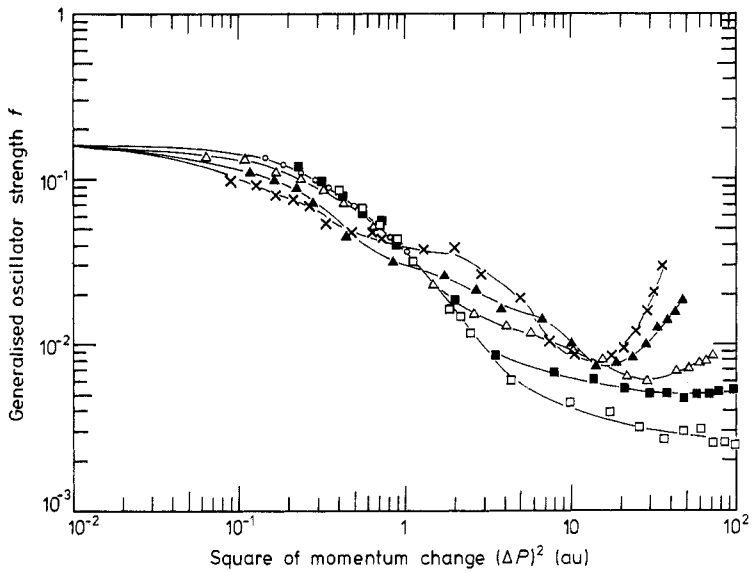

Figure 6. Generalised oscillator strength as a function of the square of momentum change (in atomic units) for the excitation of the Schumann–Runge continuum in O_2 at different electron energies: × 150 eV, ▲ 200 eV, △ 300 eV, ■ 400 eV, □ 500 eV. The small open circles ∘ indicate the experimental results of Lassettre *et al* (1964b) at E_0 = 519 eV.

This extrapolation is based on the theory of limiting oscillator strengths developed by Lassettre *et al* (1969). That is, for zero momentum transfer the limiting values of the GOS is the optical oscillator strength regardless of whether the Born approximation is valid or not (it is sometimes called Lassettre's law). The accuracy of the oscillator strength obtained here is estimated to be the same as for the DCS of the SR continuum.

4.2.3. The sum of DCS for the 9·7–12·1 eV energy-loss region. As can be seen in figure 2, in the 9·7–12·1 eV energy-loss region, two strong bands and five weak peaks are observed in good agreement with the data of Huebner *et al* (1975). These peaks correspond closely to the groupings indicated by Tanaka (1952). The 'longest band' and 'second and third bands' were observed first by Price and Collins (1935) and by Tanaka (1952), respectively. The longest band was assigned by Ogawa (1971) to the $^3\Sigma_u^-(v' = 1)$ Rydberg state and by Cartwright *et al* (1973) to the $(3p\sigma_u)^3\Pi_u$ Rydberg state. Yoshimine *et al* (1976) assigned the longest, second and third band to transitions from the ground X $^3\Sigma_g^-(v'' = 0)$ state to $v' = 0$, 1 and 2, respectively, of the E $^3\Sigma_u^-$ state (original paper B′ $^3\Sigma_u^-$ state) by means of configuration-interaction calculations. Another four weak peaks (10·76, 11·03, 11·24 and 11·46 eV) have not yet been assigned.

We obtained the sum of the DCS for the excited states ranging from 9·7 to 12·1 eV energy loss. These data are expected to be useful for the analysis of the electron slowing-down processes in the earth's atmosphere. These DCS were determined by the procedures described in §3.2 and are shown in figure 7. The DCS shows forward-peaking behaviour and has a minimum around 80–100°. This minimum moves to large angles as the collision energy decreases.

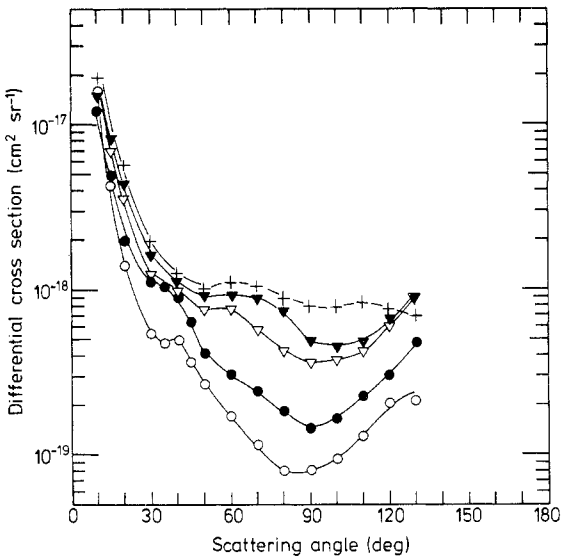

Figure 7. The sum of the DCS for excitation of the excited states in the range from 9·7 to 12·1 eV energy loss in O_2 at different incident energies; + 20 eV, ▼ 30 eV, ▽ 50 eV, ● 70 eV, ○ 100 eV.

A comparison of figure 5(*a*) with figure 7 for the same impact energy indicates that the DCS concerned here have angular distributions very similar to those for excitation of the SR continuum. Therefore, we suggest that the transitions for the excited states in the range 9·7–12·1 eV energy loss are dominated mostly by optically allowed transitions. This fact is consistent with Yoshimine's assignment, because the transition from the ground $X\ ^3\Sigma_g^-$ state to the $E\ ^3\Sigma_u^-$ state is optically allowed. We estimate the accuracy of the sum of the DCS (9·7–12·1 eV region) to be about 40%.

4.2.4. A comparison of the DCS. The present DCS at $E_0 = 20$ and 50 eV are compared with results of Trajmar *et al* (1971, 1972) at $E_0 = 20$ and 45 eV, respectively, in figures 8 and 9. In both experiments the normalisation procedures and the absolute values used as standards are very similar. As can be seen in figures 8 and 9, the present elastic DCS are smaller than the results of Trajmar *et al* on the whole but the angular distribution agree well.

This difference is supposed to be due to the difference in the extrapolation procedures for the DCS at large scattering angles. Trajmar *et al* measured relative DCS up to $\theta = 90°$, and for $\theta = 90$–$180°$ they extrapolated these relative DCS as if the DCS decrease monotonically with the scattering angle. This extrapolation yields a large normalisation constant C in equations (3) and (4). Consequently, the elastic DCS of Trajmar *et al* in figures 8 and 9 are larger than the present ones. In figure 9 the impact energy used by Trajmar *et al* is smaller by 5 eV than the present one, and so the slight increase of elastic DCS is reasonable.

The angular distributions for the SR continuum are in good agreement with the present results. The magnitude of the DCS agrees within the errors of the measurement.

4.3. Integral cross section

In figure 10 integral cross sections for the SR continuum are compared with the

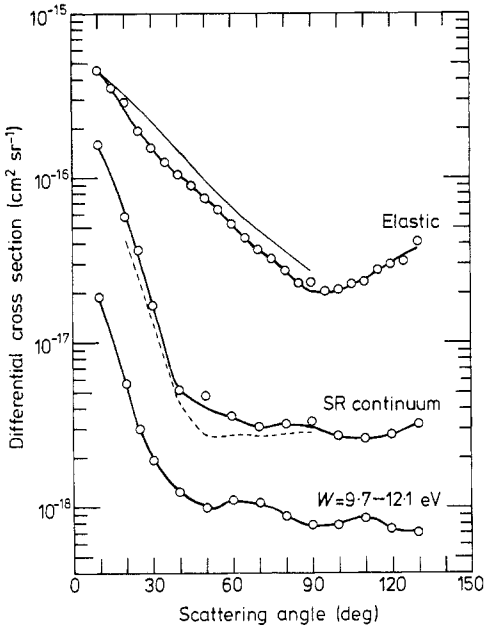

Figure 8. The DCS for elastic scattering, excitation of the Schumann–Runge continuum and the excited states in the range from 9·7 to 12·1 eV energy loss in O_2 at an incident electron energy of 20 eV. The symbol ○ and the bold curves show present results. The fine curve (elastic) and broken curve (SR continuum) indicate the experimental data of Trajmar *et al* (1971, 1972).

measured values of Trajmar *et al* (1972) and with theoretical calculations. The fine curve marked by Bethe asymptotic in figure 10 was calculated by means of the formula of the Bethe asymptotic cross section (Inokuti 1971) for optically allowed transitions

$$\sigma_{SR}(E_0) = \frac{4\pi a_0^2 Z^2}{E_0/R} \frac{f_0}{W_{SR}/R} \ln\left(\frac{4C_{SR}E_0}{R}\right)$$

where a_0 is the Bohr radius, Z the charge of incident electron ($Z = 1$), R the Rydberg energy (13·605 eV), E_0 the electron impact energy (eV), W_{SR} the excitation energy from the ground state to SR level (8·44 eV), f_0 the optical oscillator strength of the SR continuum ($f_0 = 1{\cdot}61$) and C_{SR} a constant which may be related to the angular distribution of the scattering ($C_{SR} = 1$).

Although a single energy level at 8·44 eV is postulated in this calculation and no account was taken of the width of the SR continuum, the results of this calculation agree very well with the present data. An agreement at low impact energy is, however, unexpected because this calculation does not hold at low impact energies.

In figure 11 integral cross sections for the total scattering σ_{tot}, elastic scattering σ_{elas}, total ionisation σ_{ion}, excitation of the SR continuum σ_{SR} and the excited states in the energy-loss range 9·7–12·1 eV σ_W are shown as functions of electron impact energy in O_2. From these figures and table 1, the general behaviour of integral cross sections are concluded.

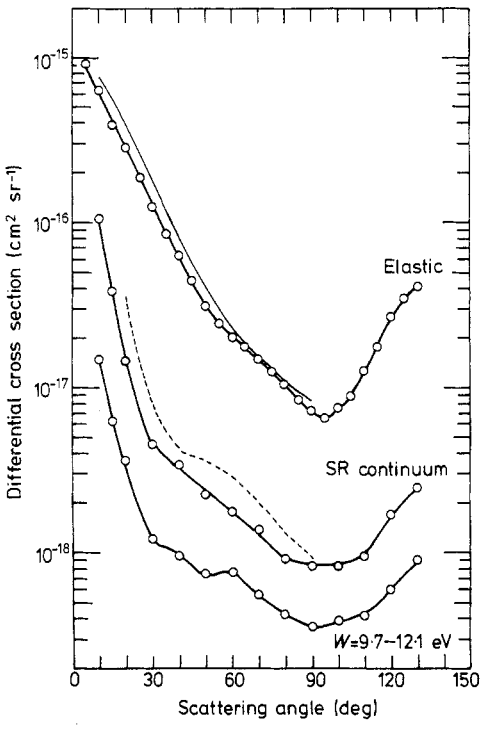

Figure 9. As figure 8, except for impact electron energies $E_0 = 50$ eV (present results) and $E_0 = 45$ eV (results of Trajmar *et al*; the fine curve and broken curve).

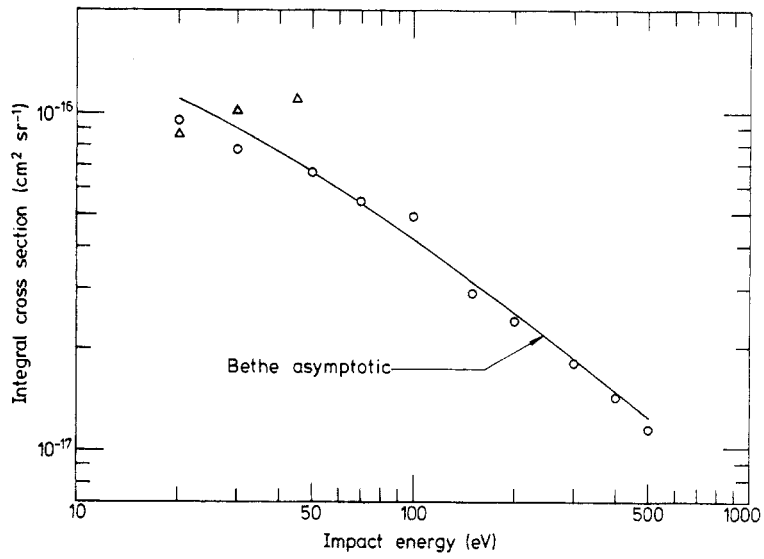

Figure 10. Integral cross sections for the Schumann–Runge continuum as a function of electron impact energy. The symbols ○ and △ indicate the present results and the measured values of Trajmar *et al* (1972), respectively. The fine curve marked by Bethe asymptotic represents the results of theoretical calculations.

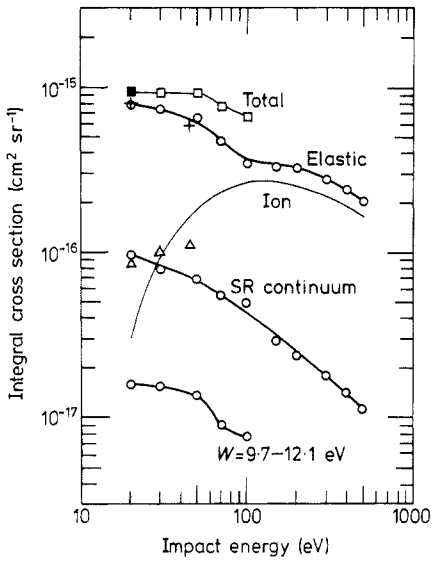

Figure 11. Integral cross sections for the total scattering, elastic scattering, total ionisation, excitation of the Schumann–Runge continuum and the excited states in the energy-loss region 9·7–12·1 eV as a function of electron energy in O_2. The symbol ○ and the bold curves show the present data. The symbols ■ and □ indicate the measured total cross sections of Salop and Nakano (1970) and Sunshine *et al* (1967), respectively. The fine curve represents the measured total ionisation cross sections of Rapp and Englander-Golden (1965). The symbols + and △ indicate the results of Trajmar *et al* (1972) for elastic scattering and excitation of the Schumann–Runge continuum, respectively.

(i) The present integral cross sections decrease as the impact energy increases in the present energy region.

(ii) The percentage contributions of the different cross sections to σ_{tot} are:

$$\sigma_{elas}: 83{\cdot}0\text{–}51{\cdot}3\%,\ \sigma_{ion}: 3{\cdot}3\text{–}40\%,\ \sigma_{SR}: 10{\cdot}1\text{–}7{\cdot}4\% \text{ and } \sigma_{W}: 1{\cdot}7\text{–}1{\cdot}1\%$$

for the impact energy range 20–100 eV.

(iii) For the impact energy range 150–500 eV, $\sigma_{elas}/\sigma_{SR} = 11 \sim 18$.

(iv) For the impact energy range 100–500 eV, σ_{elas} and σ_{ion} dominate σ_{tot}.

σ_{elas} and σ_{SR} at $E_0 = 20$, 30 and 45 eV from the measured values of Trajmar *et al* (1971, 1972) are shown in figure 11 for comparison. Their σ_{elas} agree well with the present measurements. The σ_{SR} of Trajmar *et al* rise in the 20–45 eV region, while our data show a decrease with energy. The percentage errors included in the integral cross section are given in tables 3 and 4.

Acknowledgments

The author is grateful to Professor H Suzuki, Dr T Takayanagi, Professor S Yoshida and Professor Y Kaneko for stimulating discussions and criticising the manuscript. We are also indebted to Mr A Yagishita, Mr H Oomoto, Mr A Nakashio and Miss C Hirota for their help in the measurement of the experimental data.

References

Bethe H A 1930 *Ann. Phys., Lpz.* **5** 325

Bromberg J P 1974 *J. Chem. Phys.* **60** 1717–21

Cartwright D C, Fiamengo N A, Williams W and Trajmar S 1976 *J. Phys. B: Atom. Molec. Phys.* **9** 419–25

Cartwright D C, Hunt W J, Williams W, Trajmar S and Goddard W A III 1973 *Phys. Rev.* A **8** 2436–48

Chamberlain G E, Simpson J A, Mielczarek S R and Kuyatt C E 1967 *J. Chem. Phys.* **47** 4266–7

Dillon M A and Lassettre E N 1975 *J. Chem. Phys.* **62** 2373–90

Geiger J and Schröder B 1968 *J. Chem. Phys.* **49** 740–4

Hayashi S 1975 *PhD Thesis* University of Tokyo

Hayashi S and Kuchitsu K 1976 *J. Phys. Soc. Japan* **41** 1724–32

Hudson R D 1971 *Rev. Geophys. Space Phys.* **9** 305–406

Huebner R H, Cellotta R J, Mielczarek S R and Kuyatt C E 1975 *J. Chem. Phys.* **63** 241–8

Inokuti M 1971 *Rev. Mod. Phys.* **43** 297–347

Kim Y K and Inokuti M 1968 *Phys. Rev.* **175** 176–87

Krupenie P H 1972 *J. Phys. Chem. Ref. Data* **1** 423–534

Lassettre E N, Bermann A S, Silverman S M and Krasnow M E 1964a *J. Chem. Phys.* **40** 1232–42

Lassettre E N and Francis S A 1964 *J. Chem. Phys.* **40** 1208–17

Lassettre E N, Silverman S M and Krasnow M E 1964b *J. Chem. Phys.* **40** 1261–5

Lassettre E N and Skerbele A 1971 *J. Chem. Phys.* **54** 1597–607

Lassettre E N, Skerbele A and Dillon M A 1969 *J. Chem. Phys.* **50** 1829–39

Lassettre E N, Skerbele A, Dillon M A and Ross K J 1968 *J. Chem. Phys.* **48** 5066–95

Lassettre E N, Skerbele A and Meyer V D 1966 *J. Chem. Phys.* **45** 3214–26

Ogawa M 1971 *J. Chem. Phys.* **54** 2250

Price W C and Collins G 1935 *Phys. Rev.* **48** 714–9

Rapp D and Englander-Golden P 1965 *J. Chem. Phys.* **43** 1464–79

Salop A and Nakano H H 1970 *Phys. Rev.* A **2** 127–31

Sunshine G, Aubrey B B and Bederson B 1967 *Phys. Rev.* **154** 1–8

Suzuki H, Takayanagi T and Wakiya K 1974 *Studies of Atomic Collisions and Related Topics in Japan—Progress Report* No 2 pp 15–9

Takayanagi T 1973 *PhD Thesis* Sophia University, Tokyo

Tanaka Y 1952 *J. Chem. Phys.* **20** 1728–33

Trajmar S, Cartwright D C and Hall R I 1976 *J. Chem. Phys.* **65** 5275–9

Trajmar S, Cartwright D C and Williams W 1971 *Phys. Rev.* A **4** 1482–92

Trajmar S, Williams W and Kuppermann A 1972 *J. Chem. Phys.* **56** 3759–65

Yagishita A, Takayanagi T and Suzuki H 1976 *J. Phys. B: Atom. Molec. Phys.* **9** L53–7

Yoshimine M, Tanaka K, Tatewaki H, Obara S, Sasaki F and Ohno K 1976 *J. Chem. Phys.* **64** 2254–5

Wakiya K 1978 *J. Phys. B: Atom. Molec. Phys.* **11** 3931–8

Watanabe K, Inn E C Y and Zelikoff M 1953 *J. Chem. Phys.* **21** 1026–30